Detection and Localization of Micro-Cracks in Plate Structures Using Topological Acoustic Sensing

---

GUANGDONG ZHANG, TRIBIKRAM KUNDU,
PIERRE A. DEYMIER and KEITH RUNGE

ABSTRACT

This work presents an emerging technique called topological acoustic (TA) sensing for identifying micro-cracks in plate structures. The geometric phase change – index (GPC-I) from TA sensing is defined as the damage index (DI) to indicate the presence of micro-cracks. Then a localization methodology adopting GPC-I is proposed to identify random locations of micro-cracks occurrence in plate structures. Finite element method (FEM) based analysis is carried out in Abaqus/CAE software for 1) modeling contact acoustic nonlinearity (CAN) arising from micro-cracks and 2) verifying the proposed localization method. Numerical results show that micro-cracks induced CAN can be properly generated in FEM with artificially changing the cracks' surface properties. Random locations of micro-cracks occurrence in plate structures can be identified accurately with the proposed localization method. Compared to the amplitude ratio (AR) parameter, the newly developed GPC-I can give more robust and distinguishing features for localizing micro-cracks. The velocity ratio (VR) parameter fails to capture nonlinear response arising from micro-cracks. This work is the first attempt to investigate the capability of GPC-I in capturing nonlinear response generated from micro-cracks. Such capability of GPC-I for topological acoustic sensing can provide new insight to benefit nonlinear ultrasonic community.

INTRODUCTION

Micro-cracks in engineering structural components are generally difficult to detect with commonly used linear ultrasonic (LU) techniques. Undetected micro-cracks can coalesce to form macro-cracks and result in sudden structural failures [1]. Nonlinear ultrasonic (NLU) techniques due to their high sensitivity to micro-cracks (damages at their very early stages) are becoming more popular [2]. Timely detection and localization of micro-cracks in structural components by NLU techniques hold great significance in structural health monitoring (SHM) for ensuring safe operations of engineering structures.

Detecting micro-cracks by NLU techniques relies on the acoustic nonlinearity generation from the contact and separation of two opposing surfaces of micro-cracks as the elastic wave propagates through the region containing micro-cracks. This phenomenon is referred to as contact acoustic nonlinearity (CAN) [3-5]. Micro-cracks induced CAN causes the variations of nonlinear components in amplitude spectral plots, and they can be captured by various well-established NLU techniques. Nonlinear ultrasonic techniques such as higher harmonics generation (HHG) [6], wave mixing [7], frequency modulation (FM) [8, 9] and sideband peak count (SPC)-based techniques [10-12] have been adopted for detecting micro-cracks in engineering structures. With the definition of damage indices (DIs) in those well-established NLU techniques, micro-cracks can be successfully identified and detected. The majority of available magnitude-

---

Guangdong Zhang, Tribikram Kundu, Pierre A. Deymier, Keith Runge
New Frontiers of Sound Science and Technology Center, University of Arizona, Tucson, AZ 85721, USA

based DIs in amplitude spectral plots can encounter difficulties in detecting and/or localizing micro-cracks in practical applications. For instance, Zhang et al. [13] found that some topographies such as heterogeneous plate structures can make single crack to be undetectable even with the promising magnitude-based SPC-I technique, since SPC-I is designed for detecting distributed micro-cracks. They introduced a newly developed topological acoustic (TA) sensing technique with geometric phase change (GPC) DI to overcome these issues.

For defect localization, Zhang et al. [14] initially proposed a GPC-based methodology for locating defects in both homogeneous and heterogeneous plate structures [15]. By defining the GPC-index (GPC-I) [16], it was found that defects can be identified with high sensitivity. The proposed localization methodology using GPC-I can give accurate defect location information and show superiority over commonly used acoustic parameters namely TOF-based velocity differences (VD) and magnitude-based amplitude ratio (AR) methods. However, only the linear scattering information from defects was utilized in these works by Zhang et al. [13-16], The micro-crack localization using GPC-I from the nonlinear response has not been reported yet.

This work focuses on the capability of GPC technique in sensing nonlinearity arising from micro-cracks. The GPC-I technique is also extended to identify micro-cracks' locations which has not been reported before. Finite element method (FEM) based analysis is carried out in Abaqus/CAE software for 1) modeling contact acoustic nonlinearity (CAN) arising from micro-cracks and 2) verifying the proposed localization method. The method of micro-cracks localization using GPC-I is also compared to commonly used acoustic parameters namely velocity ratio (VR) and amplitude ratio (AR).

MICRO-CRACKS LOCALIZATION METHODOLOGY USING GPC-I

The basic concepts of GPC and GPC-I have been introduced in detail in the authors' earlier publications [13-16]. Those detailed derivations of GPC and GPC-I parameters are omitted here to avoid duplication. Here, we only briefly describe the localization methodology using GPC-I. The two-dimensional (2-D) view schematic illustration of the proposed localization methodology is shown in figure 1.

First, we choose the sensor point T_1 as the transmitter as shown in figure 1a. All other sensors record displacement or velocity series generated from T_1. A number, n, of detection sensors are arranged for convenience in an arc aways from the transmitter. Here, for micro-crack localization sensing purpose we reduce the dimension (n) of the

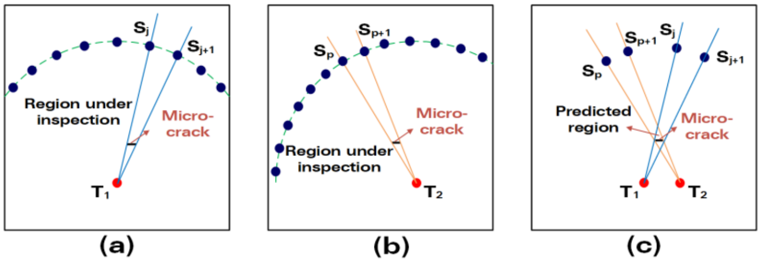

Figure 1. Schematic illustrations for the proposed localization methodology using GPC-I. The plate with a micro-crack is the perturbed state and the plate without any micro-crack (damage-free) is the reference state.

detected acoustic field state vector mentioned in topological acoustic sensing to 2 by considering two adjacent receivers (sensors *j* and *j*+1), which means that there are two components in the acoustic field state vectors. The two-dimensional (2-D) complex state vector can be constructed from the Fourier transform of the time series received by the two adjacent sensors. The normalized complex state vector for reference state (without defects) at receiving sensor *j* can be written as,

$$s_j = \frac{1}{\sqrt{a_j^2 + a_{j+1}^2}} \begin{pmatrix} a_j e^{i\phi_j} \\ a_{j+1} e^{i\phi_{j+1}} \end{pmatrix} \tag{1}$$

where *j* denotes the receiving sensor number, and *i* is the imaginary unit. a and ϕ are magnitude and spatial phase at each of the two receiving points.

Accordingly, in the perturbed state (with micro-cracks) the normalized 2-D state vector at receiving sensor *j* can be expressed as,

$$s_j' = \frac{1}{\sqrt{a_j'^2 + a_{j+1}'^2}} \begin{pmatrix} a_j' e^{i\phi_j'} \\ a_{j+1}' e^{i\phi_{j+1}'} \end{pmatrix} \tag{2}$$

The GPC at sensor number *j* is calculated in the 2-D subspace as,

$$\Delta\varphi_j(f) = \mathrm{arcos}\left(\mathrm{Re}\left(s_j{}^* \cdot s_j{}'\right)\right), \quad \Delta\varphi \in [0, \pi] \tag{3}$$

where s_j^* denotes the complex conjugate of state vector s_j at receiving sensor *j* while Re stands for the real part of a complex quantity.

The GPC-I at the receiving sensor number *j* is then calculated by averaging $\Delta\varphi_j(f)$ over a chosen frequency range. A large GPC-I value indicates likely presence of a defect along the sensing paths from the transmitter to sensor numbers *j* and *j*+1. Hence, the defect is likely located in the triangular region shown in figure 1a formed by the transmitter T_1 and the two sensors numbered *j* and *j*+1.

Next, we consider another transmitter location T_2 shown in figure 1b and determine the GPC, $\Delta\varphi_{j+n}(f)$, employing the two adjacent receiving sensor numbered *p* and *p*+1. The value of GPC-I at the receiving sensor S_p, is then used to potentially locate the defect in the triangle formed by T_2, sensors *p* and *p*+1. Large values of GPC-I for both triangles predict the defected region as the intersection of these two triangles as shown in figure 1c. In this manner the micro-crack can be localized.

NUMERICAL MODELS

In this section, numerical modeling is carried out by finite element method (FEM) using Abaqus/CAE software. The 2-D view of the problem geometry for numerical modeling is shown in figure 2. Figures 2a and 2b show the two cases for micro-crack localization when two transmitters T_1 and T_2 are used. The dimension of the plate is $200 \times 200 \times 3\mathrm{mm}^3$, and the material properties of the plate for numerical modeling are shown in Table I. The plate with a micro-crack is the perturbed state and the one without any damage is the reference state.

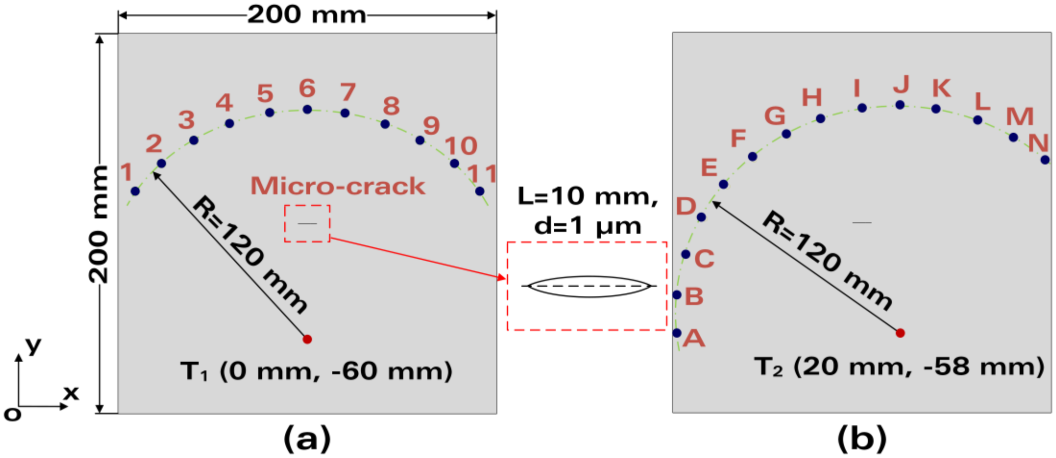

Figure 2. 2-D view of the problem geometry for micro-crack detection and localization used in the numerical modeling. (a) Transmitter is T_1 and (b) transmitter is T_2. The reference state is the plate without any micro-crack and is not shown in the figure. We use two sets of receivers arranged in arcs centered of the transmitters.

For the two-step localization methodology described in section 2, the first transmitter T_1 is arbitrarily positioned at (0 mm, -60 mm) as shown in figure 2a. Receiving sensors numbered 1 to 11 are strategically distributed on an arc with the same 120 mm radius, and this configuration can simplify the post-signal processing by maintaining constant wave propagation paths. Similarly, the transmitter T_2 is arbitrarily positioned at (20 mm, -58 mm), and receiving sensors numbered A to N are also strategically distributed on an arc with a 120 mm radius. These receiving sensors are put on the surface of the plate and the specific locations are calculated according to the coordinate system and listed in Table II. Non-contact laser Doppler vibrometer (LDV) may also be used to measure the displacement field along the detector's arcs. Center points of two micro-cracks to be localized are placed at (-20 mm, -20 mm) and (0 mm, 0 mm), respectively.

The micro-crack shown in the figure is created by an elliptical cylinder with a major axis of L=10 mm and a minor axis of d=1 µm, and it is arranged along the z-axis such that the height of the elliptical column is 3 mm (the thickness of the plate). The element in the micro-crack region is refined to 0.2 mm. The element size for other parts in the plate is 1 mm. The nonlinearity generation is modeled by hard contact and shear frictionless interface in Abaqus/CAE [3, 8, 17].

A Hanning window modulated excitation of central frequency 200 kHz with two cycles is applied in the negative z direction at transmitters T_1 and T_2 in the two-step process. At the selected receiving points, the out-of-plane velocity (in the z direction) is recorded for both the reference state and the perturbed state. The sampling frequency for recording the signals is 50 MSa/s (mega samples per second).

TABLE I. MATERIAL PROPERTIES USED FOR FEM MODELING

Parameters	Young's modulus (GPa)	Poisson's ratio	Density (kg/m³)
Values	71.50	0.33	2700.00

TABLE II. TRANSMITTER LOCATIONS AND CORRESPONDING RECEIVING SENSOR LOCATIONS (UNIT IS MM)

T_1 (0,-60)		T_2 (20,-58)			
Sensor No.	Locations (x, y)	Sensor No.	Locations (x, y)	Sensor No.	Locations (x, y)
1	(-91, 17)	A	(-99,-58)	L	(61, 54)
2	(-77, 31)	B	(-98,-38)	M	(80, 45)
3	(-59, 43)	C	(-92,-17)	N	(97, 33)
4	(-41, 52)	D	(-83, 2)		
5	(-20, 58)	E	(-71, 19)		
6	(0, 60)	F	(-57, 33)		
7	(20, 58)	G	(-39, 45)		
8	(41, 52)	H	(-21, 54)		
9	(59, 43)	I	(0, 60)		
10	(77, 31)	J	(20, 62)		
11	(91, 17)	K	(40, 60)		

NUMERICAL RESULTS

In this section, micro-crack detection with GPC is presented first to show the capacity of GPC for capturing nonlinear response. Then micro-crack localization results using GPC-index (GPC-I) parameter are shown to validate the proposed localization methodology.

MICRO-CRACK DETECTION WITH GPC – CAN ARISING FROM MICRO-CRACKS

It has been found that GPC can capture both linear and nonlinear responses from damages (cracks) [14]. In numerical modeling, a micro-crack with hard contact is said to generate CAN [3, 8, 17], and we call it a nonlinear micro-crack here. Hence, without any hard contact at the interface of the micro-crack only linear response will be generated and this type of micro-crack is referred to as a linear micro-crack. Since in practical SHM applications detecting micro-cracks in structures is related to nonlinearity generation, in this paper the capacity of GPC for capturing nonlinear response arising from micro-cracks is investigated. It is necessary to figure out and separate the effects of linear and nonlinear responses on GPC behaviors to comprehensively explore the potential of GPC for micro-cracks detection.

First, responses from a nonlinear micro-crack and a linear micro-crack are numerically compared to show how CAN affects the behaviors of GPC. Then the linear micro-crack case is compared with no micro-crack case (a healthy plate). Note that the linear micro-crack and no micro-crack will involve only linear responses. The micro-crack located at (0 mm, 0 mm) is taken as an example for micro-crack detection purpose. The recorded time domain signals at sensor number 6 for transmitter T_1 are shown in figure 3.

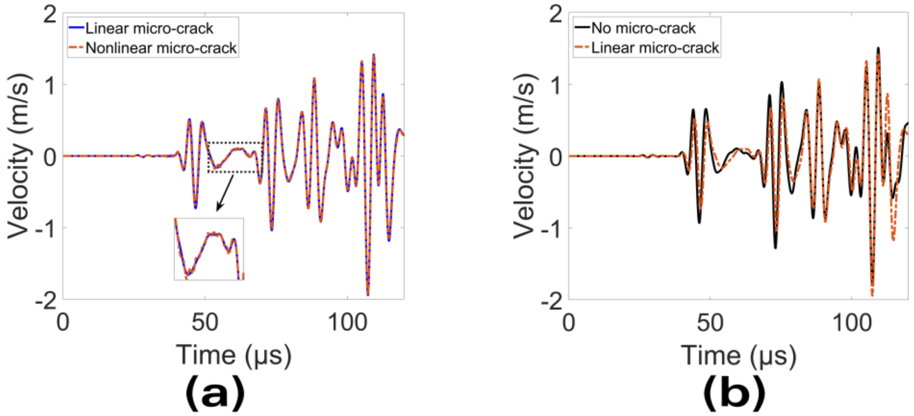

Figure 3. Time domain signals recorded at sensor 6 when transmitter is T_1 and the micro-crack is located at (0 mm, 0 mm). (a) The linear and nonlinear micro-crack cases are shown to compare the effect of nonlinearity. (b) The linear micro-crack and no micro-crack (a healthy plate) cases are shown to compare the linear responses.

For transmitter T_1 with receiving sensor number 6, the wave propagation path is perpendicular to the micro-crack. It can be seen from figure 3b that there are dynamic phase shifts but there are no wave shape distortions in the time histories when only scatterings are generated from the linear micro-crack. In figure 3a as well as in the zoomed figure, it can be observed that in the nonlinear micro-crack case (with hard contact) the time histories are slightly distorted which indicates that CAN is generated. The corresponding normalized spectral amplitude plots generated from the time histories of figure 3 are shown in figure 4.

It can be seen from figure 4a where the linear and nonlinear micro-cracks are compared that the hard contact introduced in simulation can successfully represent the presence of CAN generation. The higher harmonic components (beyond approximately 400 kHz) in nonlinear micro-crack case are much stronger and clearly observed which is not the case for the linear micro-crack case. In figure 4b, no additional frequency components are generated in linear micro-crack case in comparison to the no micro-crack case (the healthy plate). This indicates that no CAN is arising from the linear micro-crack, and the larger magnitude at higher frequency ranges in the spectral plots is due to the linear micro-crack effects from scatterings.

The frequency-dependent GPC ($\Delta\varphi$) plots for these three cases (no micro-crack, linear micro-crack and nonlinear micro-crack) at receiving sensor number 6 are shown in figure 5.

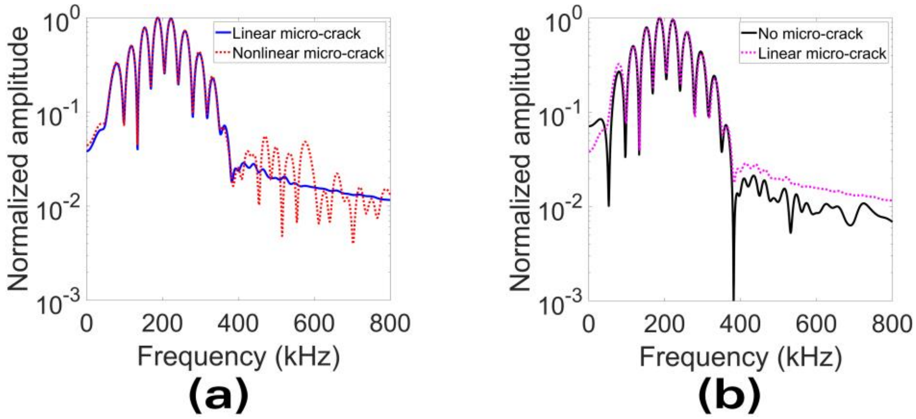

Figure 4. Normalized spectral amplitude plots corresponding to the cases investigated in figure 3.

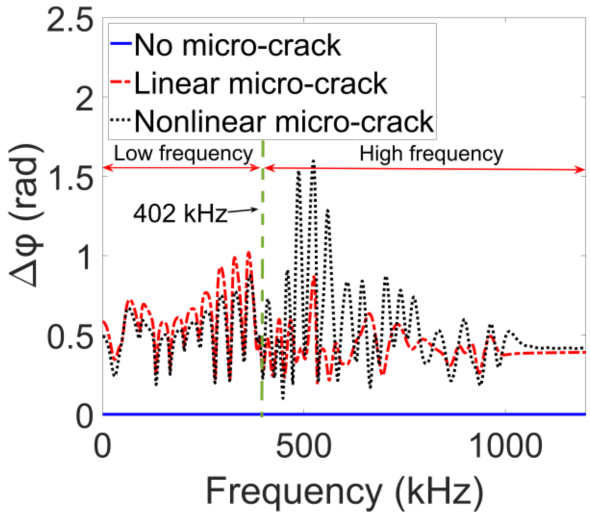

Figure 5. GPC plots at receiving sensor number 6 when transmitter is T_1 for no micro-crack, linear micro-crack and nonlinear micro-crack cases for the micro-crack located at (0 mm, 0 mm).

It can be seen from figure 5 that GPC can capture both linear and nonlinear responses from the micro-crack as variations from the healthy plate can be observed for both cases. For the nonlinear micro-crack, the GPC plots show different trends over 402 kHz frequency compared to that of the linear micro-crack. At low frequency range from 0 to approximately 402 kHz here, the GPC for linear micro-crack is larger than that corresponding to the nonlinear micro-crack. However, at high frequency range (above 402 kHz) multiple sharp additional peaks and dips are observed in the GPC plot, and these peaks are much stronger than those for the linear micro-crack case. Therefore, it can be concluded from this figure that at low frequency range the GPC captures mainly the linear scatterings from the micro-crack. At high frequency, GPC captures the nonlinear response of the micro-crack. It is suggested that in practical applications for sensing micro-cracks one should use GPC plots at the high frequency range.

MICRO-CRACK LOCALIZATION USING GPC-I

MICRO-CRACK LOCATED AT (-20 MM, -20 MM)

In section 4.1, the capability of GPC for detecting both linear and nonlinear responses arising from the micro-crack was presented. A nonlinear micro-crack can generate both linear and nonlinear responses which can be captured by the GPC parameter. In real-world SHM applications micro-cracks show strong nonlinear response while the linear scatterings can be insignificant. In general, the healthy plate is used to serve as the reference state in TA sensing. However, here to emphasize the capability of GPC for localizing micro-cracks using its pure nonlinear characteristics the linear responses are eliminated by choosing the linear micro-crack case as the reference state, while the nonlinear micro-crack case is considered as the perturbed state. Moreover, from the numerical modeling perspective, since the mesh size in the crack region has been refined, choosing the linear micro-crack as the reference state can avoid mesh discrepancies between healthy and defective models. In figure 6, we show the calculated GPC as a function of frequency for two different sensing paths when the micro-crack is located at (-20 mm, -20 mm).

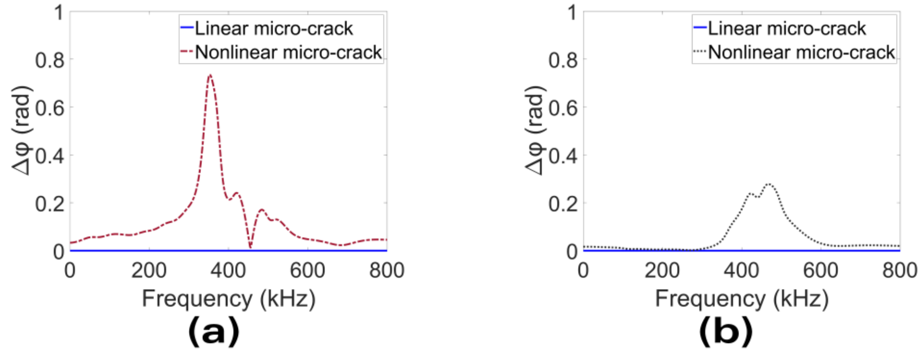

Figure 6. Calculated GPC for two sensing paths defined by sensor locations (a) 3 and (b) 6 when the transmitter is T_1 and the nonlinear micro-crack is located at (-20 mm, -20 mm).

It can be seen that over a wide frequency range (from 0 to 800 kHz) the GPC shows significantly larger values at receiving sensor 3 than that at sensor 6. This difference indicates that a defect is more likely to be present along the wave path between the transmitter T_1 and sensor 3. Then the GPC-index (GPC-I) which is the average value of GPC plots over a chosen frequency range is defined. A high value of GPC-I on a sensing path indicates a higher probability of the presence of a micro-crack on that path. With the proposed localization methodology, GPC-I at every receiving sensors should be calculated for localization purposes when transmitters are T_1 and T_2, respectively. The GPC-I plots (GPC-I vs. sensor sites) for micro-crack located at (-20 mm, -20 mm) are shown in figure 7. The GPC-I is calculated by averaging the GPC over the frequency range 0 to 800 kHz.

It can be seen from figure 7a that when T_1 is the transmitter the maximum GPC-I value is sensor site 3. Since in the proposed localization methodology the state vector is constructed with signals recorded on two adjacent sensors (two components in the state vector), GPC-I on sensor site 3 will involve the sensing paths with the two adjacent sensors 3 and 4. Therefore, the micro-crack likely occurs in the triangular area formed by connecting the transmitter T_1 and two receiving sensors 3 and 4 as shown in figure 8a. Similarly, the micro-crack is most likely located in the triangular area formed by the transmitter T_2 and receiving sensors E and F as shown in figure 8b. Then the micro-crack should be located in the quadrilateral area formed by the two triangles, as shown in figure 8c. The predicted location of the micro-crack center is (-18.79 mm, -19.05 mm) which is close to the actual location (-20 mm, -20 mm).

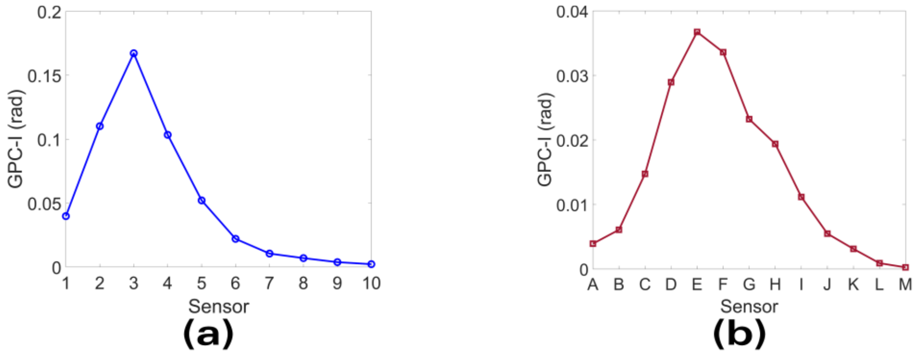

Figure 7. GPC-I plots for micro-crack located at (-20 mm, -20 mm) when transmitter is (a) T_1 and (b) T_2.

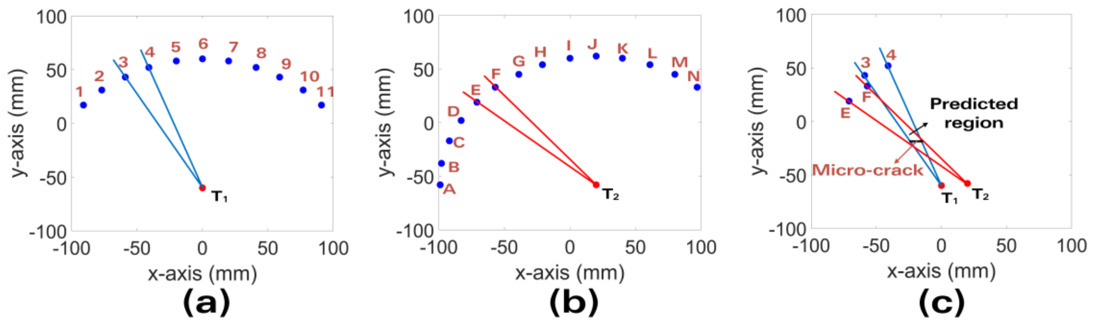

Figure 8. Micro-crack localization results using GPC-I for crack location (-20 mm, -20 mm). (a) predicted triangular region when transmitter is T_1, (b) predicted triangular region when transmitter is T_2 and (c) predicted quadrilateral region where micro-crack should be located.

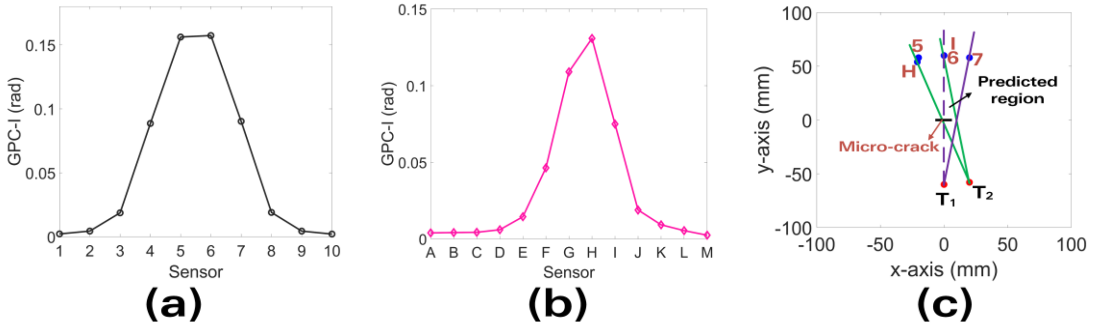

Figure 9. Micro-crack localization results using GPC-I for crack location (0 mm, 0 mm). (a) the GPC-I plot when transmitter is T_1, (b) the GPC-I plot when transmitter is T_2 and (c) predicted region where micro-crack is located.

MICRO-CRACK LOCATED AT (0 MM, 0 MM)

Similar localization process is applied for the micro-crack located at (0 mm, 0 mm) and relevant results are shown in figure 9.

Figure 9a gives the GPC-I plot (GPC-I values vs. sensor sites) when the transmitter is T_1. It is interesting to observe that the entire GPC-I plot is symmetric and the maximum GPC-I values occur on both sensor sites 5 and 6 (two sites will involve three sensors – 5, 6 and 7). In the numerical model, the transmitter T_1 is on the central line (the y-axis) and all receiving sensors are also symmetric about the y-axis. Therefore, it can be concluded from the symmetric GPC-I plot that the micro-crack is symmetric about the y-axis. With the help of the combined information in figures 9a and 9b, the predicted location of the micro-crack is shown in figure 9c. The predicted location of the micro-crack center is (0 mm, -1.68 mm) which is close to the actual location (0 mm, 0 mm).

COMPARISON RESULTS OF MICRO-CRACK LOCALIZATION USING OTHER ACOUSTIC PARAMETERS

MICRO-CRACK LOCALIZATION USING VELOCITY RATIO (VR) PARAMETER

The VR plots (VR values vs. sensor sites) for the micro-crack located at (-20mm, -20 mm) and (0 mm, 0mm) are shown in figures 10 and 11.

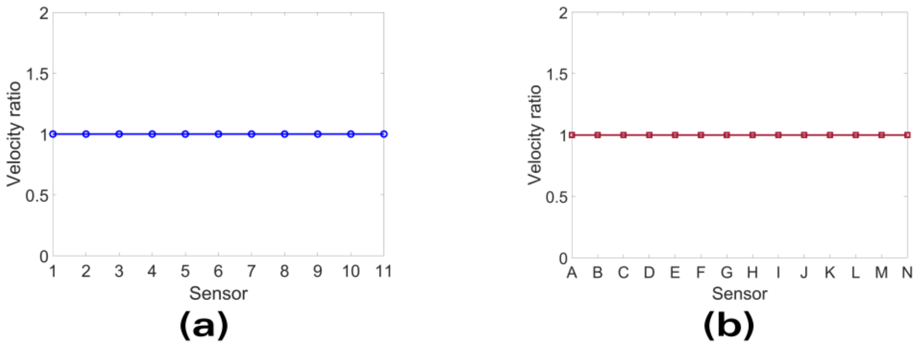

Figure 10. Micro-crack localization results using VR for location (-20 mm, -20 mm). (a) the VR plot when transmitter is T_1 and (b) the VR plot when transmitter is T_2.

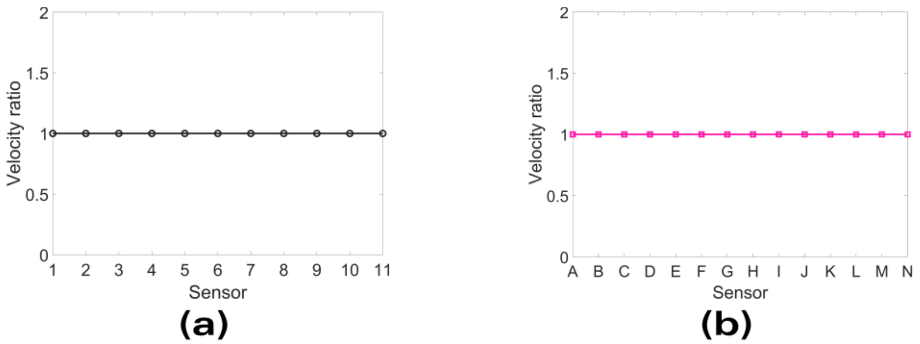

Figure 11. Micro-crack localization results using VR for location (0 mm, 0 mm). (a) the VR plot when transmitter is T_1 and (b) the VR plot when transmitter is T_2.

It can be seen from figures 10 and 11 that VR plots do not show any variations, and this indicates that the VR parameter cannot capture the nonlinear response arising from the micro-crack and is therefore not useful for localization.

MICRO-CRACK LOCALIZATION USING AMPLITUDE RATIO (AR) PARAMETER

The magnitude-based amplitude ratio (AR) parameter is calculated from the ratio of the maximum spectral amplitude values between the perturbed and reference states for each sensor site and each transmitter location and is used for micro-crack localization. The related localization results for the micro-crack located at (-20mm, -20 mm) and (0 mm, 0mm) are shown in figures 12 and 13.

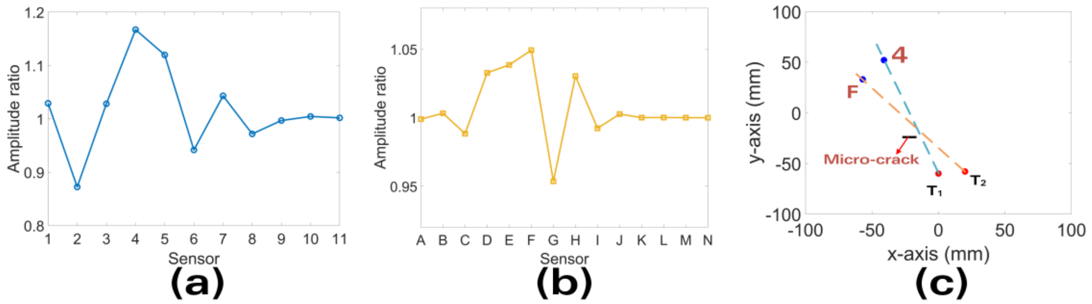

Figure 12. Micro-crack localization results using AR for location (-20 mm, -20 mm). (a) the AR plot when transmitter is T_1, (b) the AR plot when transmitter is T_2 and (c) predicted location of the micro-crack (intersection point of the two dashed lines).

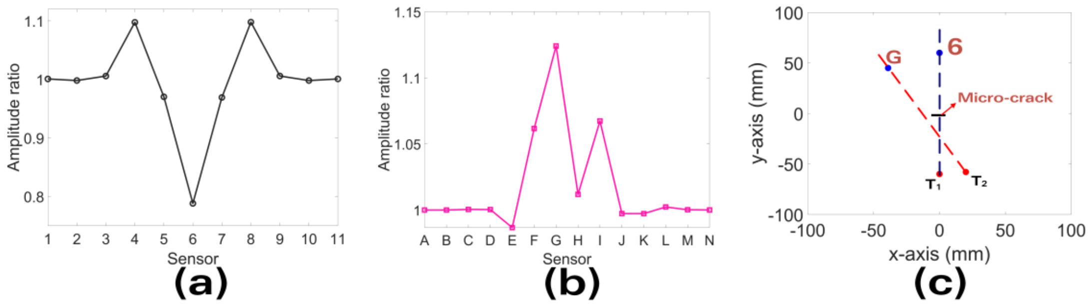

Figure 13. Micro-crack localization results using AR for location (0 mm, 0 mm). (a) the AR plot when transmitter is T_1, (b) the AR plot when transmitter is T_2 and (c) predicted location of the micro-crack (intersection point of the two dashed lines).

It can be seen from figure 12a that there is a sharp peak at receiving sensor 4 and multiple small peaks and dips (oscillations) at other receiving sensors when transmitter is T1. Since there are multiple oscillations in the AR plots in figures 12a and 12b, it is difficult to figure out the reliable sensing paths. The predicted sensing paths thus are considered as unreliable here and are denoted as dashed lines as shown in figure 12c. It can be also seen from figures 13a and 13b that there are multiple relatively large peaks in AR plots (AR values vs. sensor sites) that can make the prediction of the micro-crack uncertain, which indicates unreliable sensing paths (denoted as dashed lines in figure 13c).

CONCLUSIONS

In this work, the detection and localization of micro-cracks using the newly developed geometric phase change (GPC) parameter is investigated. The CAN effect arising from micro-crack is successfully modeled with hard contact constraints in Abaqus/CAE software. It is found that GPC has the capacity to capture the nonlinear response from the micro-crack and can subsequently detect the presence of the defect. The GPC-index (GPC-I) is defined and a modality for locating the micro-cracks is proposed. Compared to the magnitude-based amplitude ratio (AR) parameter, we show that the newly developed GPC-I approach for localizing micro-cracks is more robust. The TOF-based velocity ratio (VR) parameter fails to capture the nonlinear response arising from micro-cracks. This work is the first attempt to achieve micro-crack detection and localization using the nonlinear features of highly sensitive GPC-I parameter. The capacity of GPC for capturing nonlinear response from micro-cracks is comprehensively explored. This investigation can provide promising guidance in real-world SHM applications when using GPC for micro-cracks detection and localization.

ACKNOWLEDGEMENT

This work was partially supported by the National Science Foundation sponsored “New Frontiers of Sound Science and Technology Center” at the University of Arizona (Grant No. 2242925).

REFERENCES

1. Zhang G, Li X, Zhang S, et al. Sideband peak count-index technique for monitoring multiple cracks in plate structures using ordinary state-based peri-ultrasound theory. The Journal of the Acoustical Society of America, 2022, 152(5): 3035-3048.
2. Zhang G, Li X, Kundu T. Ordinary state-based peri-ultrasound modeling to study the effects of multiple cracks on the nonlinear response of plate structures. Ultrasonics, 2023, 133: 107028.
3. Wan X, Zhang Q, Xu G, et al. Numerical simulation of nonlinear Lamb waves used in a thin plate for detecting buried micro-cracks. Sensors, 2014, 14(5): 8528-8546.
4. Lee Y F, Lu Y. Advanced numerical simulations considering crack orientation for fatigue damage quantification using nonlinear guided waves. Ultrasonics, 2022, 124: 106738.
5. Hong M, Su Z, Wang Q, et al. Modeling nonlinearities of ultrasonic waves for fatigue damage characterization: Theory, simulation, and experimental validation. Ultrasonics, 2014, 54(3): 770-778.
6. Xu W, Su Z, Radzieński M, et al. Nonlinear pseudo-force in a breathing crack to generate harmonics. Journal of Sound and Vibration, 2021, 492: 115734.
7. Guan L, Zou M, Wan X, et al. Nonlinear Lamb wave micro-crack direction identification in plates with mixed-frequency technique. Applied Sciences, 2020, 10(6): 2135.
8. Xu X, Ai X, Liu T, et al. Microcrack Localization and Evaluation Using Nonlinear Lamb Wave-Mixing Technique and Lamb Transformer Network. IEEE Sensors Journal, 2023, 23(16): 18423-18433.
9. Klepka A, Staszewski W J, Jenal R B, et al. Nonlinear acoustics for fatigue crack detection–experimental investigations of vibro-acoustic wave modulations. Structural Health Monitoring, 2012, 11(2): 197-211.
10. Zhang G, Li X, Li T, et al. Monitoring Elastoplastic Deformation in Ductile Metallic Materials Using Sideband Peak Count-Index Technique. Journal of Nondestructive Evaluation, Diagnostics and Prognostics of Engineering Systems, 2023, 6(3).
11. Zhang G, Hu B, Alnuaimi H, et al. Numerical modeling with experimental verification investigating the effect of various nonlinearities on the sideband peak count-index technique. Ultrasonics, 2024, 138: 107259.
12. Sun M, Zhang S, Zhang G, et al. Detection and evaluation of fatigue cracks using a nonlinear ultrasonic sideband peak count technique with a pulse-echo experimental method. Journal of Sound and Vibration, 2024, 583: 118429.
13. Zhang G, Deymier P A, Runge K, et al. Monitoring damage growth and topographical changes in plate structures using sideband peak count-index and topological acoustic sensing techniques. Ultrasonics, 2024, 141: 107354.
14. Zhang G, Kundu T, Deymier P A, et al. Defect localization in plate structures using the geometric phase of Lamb waves. Ultrasonics, 2025, 145: 107492.
15. Zhang G, Kundu T, Deymier P A, et al. Defect localization in heterogeneous plate structures using the geometric phase change–index of Lamb waves. Ultrasonics, 2025: 107654.
16. Zhang G, Kundu T, Deymier P A, et al. A Comparative Study of Geometric Phase Change-and Sideband Peak Count-Based Techniques for Monitoring Damage Growth and Material Nonlinearity. Sensors, 2024, 24(20): 6552.
17. Yin S, Xiao H, Xu C, et al. Microcrack localization using nonlinear Lamb waves and cross-shaped sensor clusters. Ultrasonics, 2022, 124: 106770.